Inorganica Chimica Acta 538 (2022) 120974

Contents lists available at ScienceDirect

Inorganica Chimica Acta

journal homepage: www.elsevier.com/locate/ica

# Supramolecular aggregation of lead(II) perchlorate and a thiosemicarbazide derivative linked by a myriad of non-covalent interactions

Isabel García-Santos [a], Alfonso Castiñeiras [a], Ghodrat Mahmoudi [b,*], Maria G. Babashkina [c], Ennio Zangrando [d], Rosa M. Gomila [e], Antonio Frontera [e,*], Damir A. Safin [f,g,h,*]

[a] Departamento de Química Inorgánica, Facultad de Farmacia, Universidad de Santiago de Compostela, E-15782 Santiago de Compostela, Spain
[b] Department of Chemistry, Faculty of Science, University of Maragheh, P.O. Box 55181-83111, Maragheh, Iran
[c] Institute of Condensed Matter and Nanosciences, Université Catholique de Louvain, Place L. Pasteur 1, 1348 Louvain-la-Neuve, Belgium
[d] Department of Chemical and Pharmaceutical Sciences, University of Trieste, Via L. Giorgieri 1, 34127 Trieste, Italy
[e] Department of Chemistry, Universitat de les Illes Balears, Crta de Valldemossa km 7.5, 07122 Palma de Mallorca (Baleares), SPAIN
[f] «Advanced Materials for Industry and Biomedicine» Laboratory, Kurgan State University, Sovetskaya Str. 63/4, 640020 Kurgan, Russian Federation
[g] Innovation Center for Chemical and Pharmaceutical Technologies, Ural Federal University named after the First President of Russia B.N. Yeltsin, Mira Str. 19, Ekaterinburg 620002, Russian Federation
[h] University of Tyumen, Volodarskogo Str. 6, 625003 Tyumen, Russian Federation

ARTICLE INFO

*Keywords:*
Tetrel bond
Lead(II)
Crystal structure
X-ray crystallography
DFT calculations
QTAIM analysis

ABSTRACT

In this work, we report on a new lead(II) coordination complex $[Pb_2L_2(CH_3CN)(ClO_4)_2]\cdot 2H_2O$ (**1**·$2H_2O$), which was readily synthesized from a mixture of $Pb(ClO_4)_2\cdot 3H_2O$ and 1-(pyridine-2-yl)benzylidene-4-phenyl-thiosemicarbazide (**HL**). The crystal structure analysis of **1**·$2H_2O$ evidenced that the lead(II) cation is *N,N',S*-chelated by the tridentate pincer type **L** with formation of a $[PbL]^+$ coordination species, which dimerizes through a couple of reciprocal bridging Pb–S bonds, yielding the $[Pb_2L_2]^{2+}$ complex cation. The metal centers within this cation are linked by two Pb•••N tetrel bonds through the bridging acetonitrile molecule with the formation of a $[Pb_2L_2(CH_3CN)]^{2+}$ building unit. These units are glued by reciprocal Pb•••S tetrel bonds, yielding a 1D supramolecular polymeric chain. The lead(II) cations interact also with disordered oxygen atoms of both the minor and major occupancies of the perchlorate anions either through covalent Pb–O bonds or Pb•••O tetrel bonds, respectively. 1D polymeric chains resemble an expanded hexagonal projection and span along the *a* axis, yielding a grid-like crystal packing, where the cavities are filled by lattice water molecules. The interactions have been studied using DFT calculations and characterized by using the quantum theory of atoms-in-molecules (QTAIM) and the non-covalent interaction plot (NCIplot) computational tools.

## 1. Introduction

Design and synthesis of metal–organic coordination compounds and polymers is continuously under investigation not only for their structural diversity, but also for interesting physicochemical properties, leading to potential applications as important solid-state materials [1–6]. A key component in such compounds is represented by polydentate organic ligands that dictate the solid state architecture of the resulting metal–organic coordination compounds and most of their properties. Flexible thiosemicarbazide scaffolds and their derivatives with diverse coordination modes are good candidates because they may act as chelating/bridging ligands through their nitrogen and sulfur atoms [7]. Moreover, thiosemicarbazide molecules are used in new drug discovery [8] and for preparing several heterocycles [9,10]. They also show interesting biological properties, such as anticancer [8], antibacterial [11–13], antiviral [14,15] and antifungal [16] activities. The chemistry of lead is widely studied not only for its toxicity [17–19]. In fact, lead(II) cation possesses a very large radius and variable coordination numbers. Moreover, two decades ago the stereochemical activity of the lone pair in lead(II) compounds retrieved in the Cambridge

* Corresponding author at: «Advanced Materials for Industry and Biomedicine» Laboratory, Kurgan State University, Sovetskaya Str. 63/4, 640020 Kurgan, Russian Federation (D.A. Safin).
*E-mail addresses:* ghodratmahmoudi@gmail.com (G. Mahmoudi), toni.frontera@uib.es (A. Frontera), damir.a.safin@gmail.com (D.A. Safin).

https://doi.org/10.1016/j.ica.2022.120974
Received 17 January 2022; Received in revised form 22 March 2022; Accepted 16 April 2022
Available online 20 April 2022

Structural Database (CSD) was analyzed by using theoretical calculations [20]. This study pointed out that the coordination sphere of the lead(II) cation can be classified as holo- and hemidirected. Holodirected lead(II) complexes exhibit the coordination bonds throughout the surface of the encompassing globe. Contrariwise, hemidirected lead(II) complexes present the coordination bonds only as a part of an encompassing globe [20]. Some of us and others [21–33] have demonstrated that hemidirected lead(II) complexes have a strong tendency to form non-covalent tetrel bonding interactions and semicoordination bonds. *Tetrel bonding interactions* are non-covalent bonds between any electron rich moiety and a Lewis acid atom belonging to group 14 of elements.

Considering the above facts and in continuation of our interest in non-covalent interactions in lead(II) compounds, in this work we report the synthesis, spectroscopic characterization and X-ray analysis of a new lead(II) coordination complex of formula $[Pb_2L_2(CH_3CN)(ClO_4)_2]\cdot 2H_2O$ (**1**·$2H_2O$), that was readily synthesized by reacting $Pb(ClO_4)_2\cdot 3H_2O$ and 1-(pyridine-2-yl)benzylidene-4-phenylthiosemicarbazide (**HL**). The lead (II) cation, *N*,*N*',*S*-chelated by the tridentate pincer type **L**, forms a $[PbL]^+$ coordination species that dimerizes through a couple of reciprocal bridging Pb–S bonds yielding a $[Pb_2L_2]^{2+}$ complex cation (Scheme 1). The latter is stabilized by two Pb•••N tetrel bonds realized between the metal centers and a bridging acetonitrile molecule with formation of a $[Pb_2L_2(CH_3CN)]^{2+}$ building unit. The non-covalent and coordination bonds have been assessed and characterized with the quantum theory of atoms-in-molecules (QTAIM) [34] and the noncovalent interaction plot (NCIplot) [35] computational tools.

## 2. Experimental and theoretical methods

### 2.1. Physical measurements

The ATR-FTIR spectrum was obtained with a Varian 670 FTIR spectrometer. The $^1$H NMR spectrum in DMSO-$d_6$ was recorded with a Bruker DPX FT/NMR-400 spectrometer. Microanalyses were performed using a LECO-elemental analyzer.

### 2.2. Synthesis

A solution of **HL** (25 mg, 0.08 mmol) and $Pb(ClO_4)_2\cdot 3H_2O$ (38 mg, 0.08 mmol) in MeOH/$CH_3CN$ (40 mL, 1:1) was left undisturbed for slow evaporation. Yellow prism-like crystals were formed during the next few days and were kept in the mother liquor to avoid loss of crystallinity due to desolvation. Anal. calc. for $C_{40}H_{33}Cl_2N_9O_8Pb_2S_2$ (1317.18) (%): C 36.47, H 2.53 and N 9.57; found: C 36.18, H 2.44 and N 9.48.

### 2.3. Single-crystal X-ray diffraction

Diffraction data were collected at 100(2) K, using a Bruker D8 VENTURE PHOTON III-14 diffractometer with Mo-Kα radiation (λ = 0.71073 Å). Cell refinement, indexing, and scaling of the data sets were performed using the program Bruker Smart Apex and Saint packages [36]. An empirical absorption correction was applied to the data set [37]. The structure was solved by direct methods with SHELXS-2013 [38]. Non-hydrogen atoms were refined by full-matrix least-squares on $F^2$ with anisotropic displacement parameters using the SHELXL-2013 [38]. The Fourier map revealed the perchlorate oxygen atoms disordered over two positions with refined occupancies of 0.644(11)/0.356 (11). In addition, three residuals were interpreted as disordered water molecules with fixed occupancies of 0.5/0.25/0.25, of which those at 0.25 isotropically refined, and no H-atoms were assigned. The acetonitrile molecule is located on a two-fold axis. The contribution of H-atoms at calculated positions was included in the final cycles of refinements.

**Crystal data:** $C_{40}H_{33}Cl_2N_9O_{10}Pb_2S_2$, $M_r$ = 1349.15 g mol$^{-1}$, monoclinic, space group *I*2/a, $a$ = 10.2452(7), $b$ = 23.6331(15), $c$ = 21.6395 (17) Å, $\beta$ = 92.977(2)°, $V$ = 5232.4(6) Å$^3$, $Z$ = 4, $\rho$ = 1.713 g cm$^{-3}$, $\mu$(Mo-Kα) = 6.666 mm$^{-1}$, reflections: 171,148 collected, 6497unique, $R_{int}$ = 0.0577, $R_1$(all) = 0.0539, w$R_2$(all) = 0.1138, $S$ = 1.065.

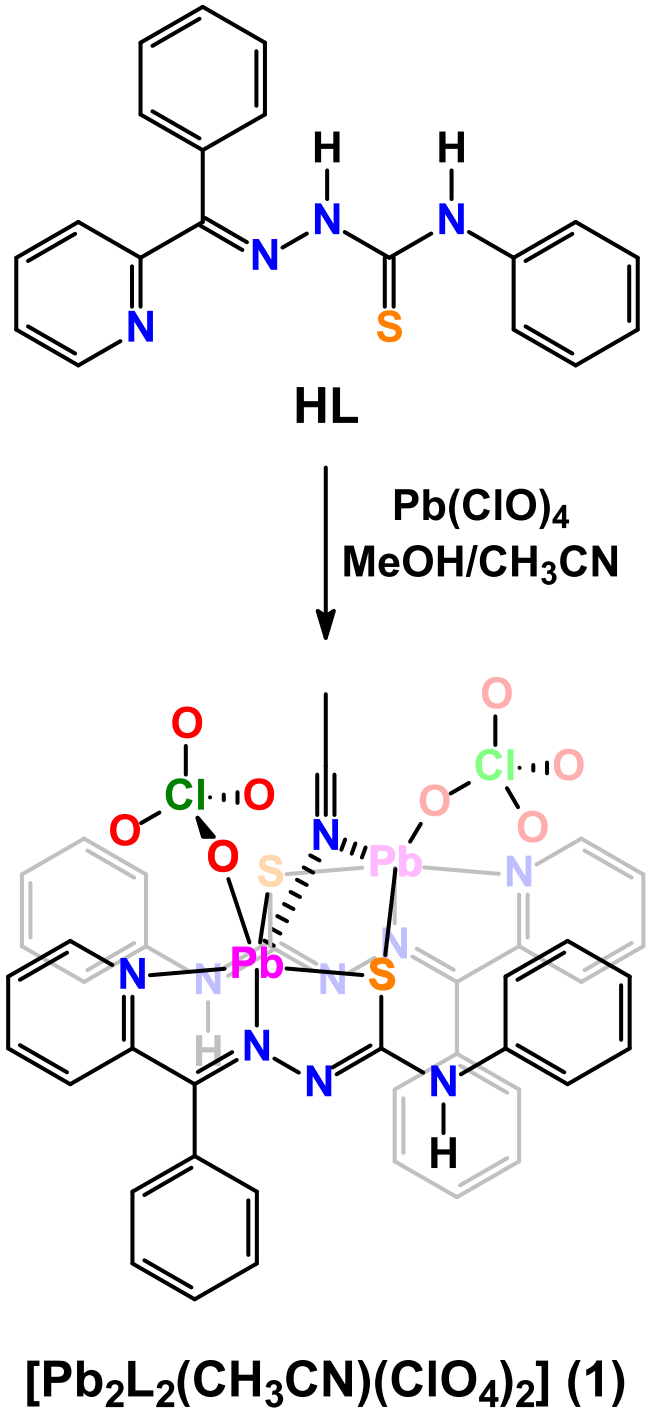


**Scheme 1.** Synthesis of complex **1**.

CCDC 2,100,674 contains the supplementary crystallographic data. These data can be obtained free of charge via https://www.ccdc.cam.ac.uk/conts/retrieving.html, or from the Cambridge Crystallographic Data Centre, 12 Union Road, Cambridge CB2 1EZ, UK; fax: (+44) 1223–336-033; or e-mail: deposit@ccdc.cam.ac.uk.

### 2.4. Theoretical calculations

The non-covalent interactions were analysed energetically using Gaussian-16 [39] at the PBE0-D3/def2-TZVP level of theory. The binding energies have been corrected using the Boys and Bernardi

counterpoise method [40]. The Grimme's D3 dispersion correction has also been used in the calculations [41]. To evaluate interactions in the solid state, the crystallographic coordinates were used and only the position of the hydrogen atoms has been optimized. This methodology and level of theory have previously been used to analyse non-covalent interactions in the solid state [42]. The interaction energies were estimated by calculating the difference between the energies of the isolated monomers and those of their assembly. The QTAIM analysis [43] and NCIplot index [44] have been computed at the same level of theory by means of the AIMAll program [45].

## 3. Results and discussion

Complex **1**·2$H_2O$ was obtained as yellow X-ray suitable plate-like crystals by slow evaporation of the solvent from a solution of **HL** and $Pb(ClO_4)_2$·3$H_2O$ in MeOH/$CH_3CN$ (Scheme 1). Isolation of the crystals from the mother liquor leads to their destruction due to the loss of lattice solvent molecules in a fairly short time. This is also reflected in the experimental elemental analysis data, which best fit to the $[Pb_2L_2(CH_3CN)(ClO_4)_2]$ composition, thus indicating a high volatility of the crystallization water molecules.

The FTIR spectrum of **1**·2$H_2O$ contains an intense band at about 1070 $cm^{-1}$ corresponding to the $ClO_4^-$ stretching vibrations, while the broad bands centered at about 3050, 3330 and 3600 $cm^{-1}$ are due to the CH, NH and $H_2O$ vibrations, respectively (Fig. 1). The acetonitrile molecule is mainly visible in the FTIR spectrum as an intense band at about 1430 $cm^{-1}$, while the band for the CN vibration is likely of low intensity and cannot be nicely distinguished from the baseline (Fig. 1).

The $^1$H NMR spectrum of **1**·2$H_2O$ was recorded in DMSO-$d_6$ and contains a single set of signals corresponding to the **L** and $CH_3CN$ ligands. Particularly, the spectrum contains a singlet at 2.05 ppm, corresponding to the acetonitrile protons (Fig. 2). The ligand **L** shows signals corresponding to the aromatic rings and NH protons. The protons of the pyridyl fragment were observed as two triplets at 6.73 and 7.98 ppm, and two doublets at 7.15 and 8.88 ppm, while the phenyl protons were observed as one triplet at 6.86 ppm, two doublets at 7.20 and 7.32 ppm and one multiplet at 7.51–7.68 ppm (Fig. 2). Finally, the NH proton was found as a singlet at 9.37 ppm (Fig. 2).

Complex **1**·2$H_2O$ crystallizes in monoclinic space group *I*2/*a* and the asymmetric unit consists of one $[PbL(CH_3CN)_{0.5}(ClO_4)]$ complex unit, with the acetonitrile molecule located on a two-fold axis and with the perchlorate oxygen atoms disordered over two positions with refined occupancies of 0.644(11)/0.356(11), and one molecule of water, which is disordered with fixed occupancies of 0.5/0.25/0.25, of which those at 0.25 isotropically refined, and no H-atoms assigned (Fig. 3).

The lead(II) cation is *N*,*N*',*S*-coordinated by the deprotonated tridentate pincer type chelating **L** with comparable Pb1–N1 and Pb1–N2

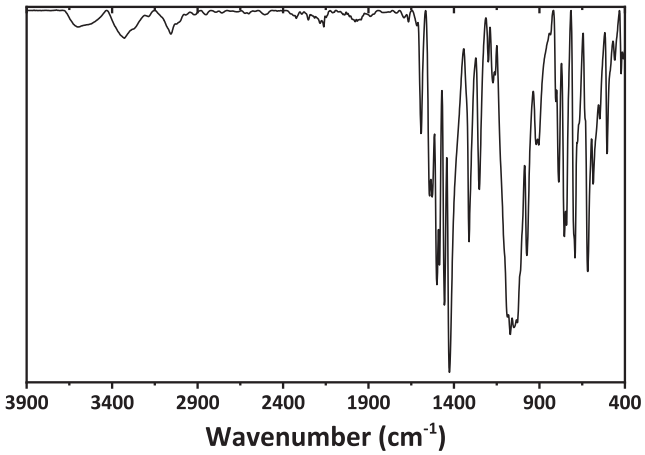


**Fig. 1.** The FTIR spectrum of complex **1**·2$H_2O$.

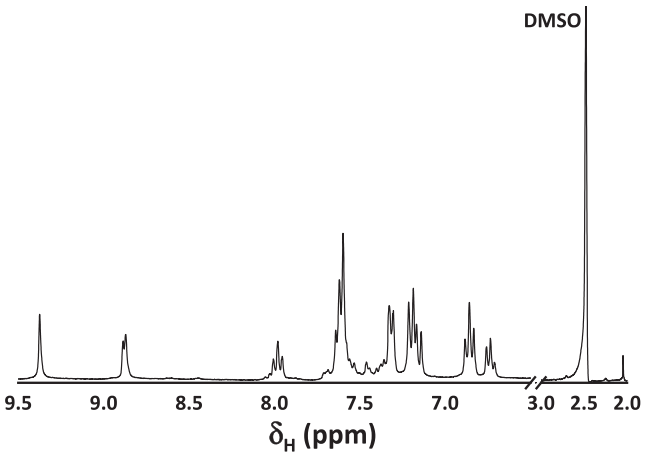


**Fig. 2.** The $^1$H NMR spectrum of complex **1**·2$H_2O$ recorded in DMSO-$d_6$.

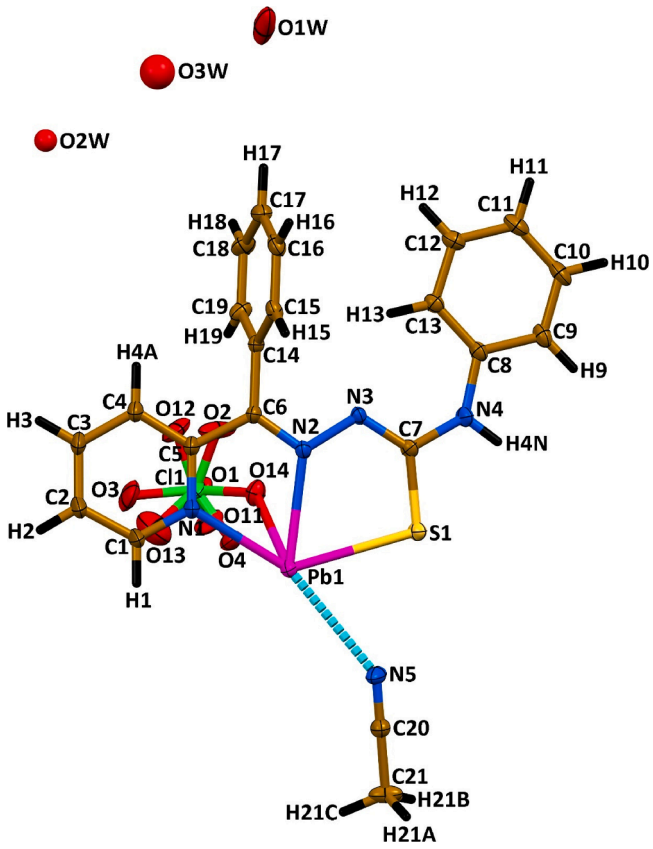


**Fig. 3.** The crystallographic asymmetric unit of complex **1**·2$H_2O$ (the dashed cyan line indicates the Pb•••N tetrel bond).

bond lengths of 2.511(7) and 2.538(5) Å (Table 1). The Pb1–S1 bond distance is of 2.8312(16) Å, with the sulfur acting as a bridging atom (Fig. 3). The complex is located about a two-fold axis and the symmetry related Pb1–S1_a bond of 2.7999(11) Å is responsible for the formation of the dimeric dinuclear cationic species $[Pb_2L_2(CH_3CN)]^{2+}$ (Fig. 4). Thus, the two deprotonated ligands **L** are head-to-tail located with respect to the $Pb_2S_2$ core and their mean planes form a dihedral angle of about 25°. Moreover, the $Pb_2S_2$ moiety shows a puckered conformation (Fig. 4) and the dihedral angle between the $PbS_2$ fragments is calculated to be 27.5° with the Pb1•••Pb1_a separation of 4.0439(6) Å. The observed dinuclear configuration with facing ligands **L** is likely affected by packing requirements but the acetonitrile molecule appears to have a

**Table 1**
Selected bond lengths (Å) and angles (°) for complex **1**·2$H_2O$.

| | | | |
|---|---|---|---|
| *Bond lengths*[a] | | | |
| Pb1–N1 | 2.511(7) | Pb1•••O4 | 3.145(9) |
| Pb1–N2 | 2.538(5) | Pb1•••O4$^{\#3}$ | 3.170(9) |
| Pb1•••N5 | 2.982(7) | Pb1•••Pb1_a$^{\#1}$ | 4.0439(6) |
| Pb1–S1 | 2.8312(16) | C5–C6 | 1.487(9) |
| Pb1–S1_a$^{\#1}$ | 2.7999(16) | C6–N2 | 1.293(8) |
| Pb1•••S1_b$^{\#2}$ | 3.3873(16) | C7–N3 | 1.299(8 |
| Pb1–O11_c$^{\#3}$ | 2.764(16) | C7–N4 | 1.361(9) |
| Pb1–O14 | 2.819(13) | N2–N3 | 1.380(6) |
| Pb1•••O1$^{\#3}$ | 3.178(8) | C7–S1 | 1.762(7) |
| *Bond angles*[a] | | | |
| S1–Pb1–N1 | 131.98(16) | N2–Pb1–O14 | 63.2(3) |
| S1–Pb1–N2 | 67.68(10) | N2–Pb1–S1_a | 84.50(12) |
| S1–Pb1•••N5 | 68.82(9) | N2–Pb1•••S1_b | 120.05(12) |
| S1–Pb1–O14 | 90.4(3) | N2–Pb1–O11_c | 145.4(3) |
| S1–Pb1–S1_a | 84.67(5) | N5•••Pb1–O14 | 138.6(3) |
| S1–Pb1•••S1_b | 76.69(4) | N5•••Pb1–S1_a | 69.22(9) |
| S1–Pb1–O11_c | 145.8(3) | N5•••Pb1•••S1_b | 69.81(8) |
| N1–Pb1–N2 | 64.79(19) | N5•••Pb1–O11_c | 77.6(4) |
| N1–Pb1•••N5 | 145.7(2) | O14–Pb1–S1_a | 146.6(3) |
| N1–Pb1–O14 | 74.5(4) | O14–Pb1•••S1_b | 70.8(3) |
| N1–Pb1–S1_a | 84.5(2) | O14–Pb1–O11_c | 111.6(5) |
| N1–Pb1•••S1_b | 134.7(2) | S1_a–Pb1•••S1_b | 138.78(4) |
| N1–Pb1–O11_c | 80.7(4) | S1_a–Pb1–O11_c | 89.8(4) |
| N2–Pb1•••N5 | 130.60(16) | S1_b•••Pb1–O11_c | 85.8(3) |
| *Dihedral angles*[b] | | | |
| PbNCCN•••PbNNCS | 3.96 | PbNNCS•••Ph(NH) | 4.00 |
| PbNCCN•••Py | 11.22 | PbNNCS•••Ph | 81.47 |
| PbNCCN•••Ph(NH) | 3.74 | Py•••Ph(NH) | 7.8(5) |
| PbNCCN•••Ph | 84.92 | Py•••Ph | 78.3(5) |
| PbNNCS•••Py | 11.38 | Ph(NH)•••Ph | 81.8(3) |

[a] Symmetry codes: #1 1/2 – *x*, *y*, 1 – *z*; #2 1 – *x*, –*y*, 1 – *z*; #3 –1/2 + *x*, –*y*, *z*.
[b] Dihedral angles between the least-square planes, formed by the corresponding aromatic rings within the ligand **L**.

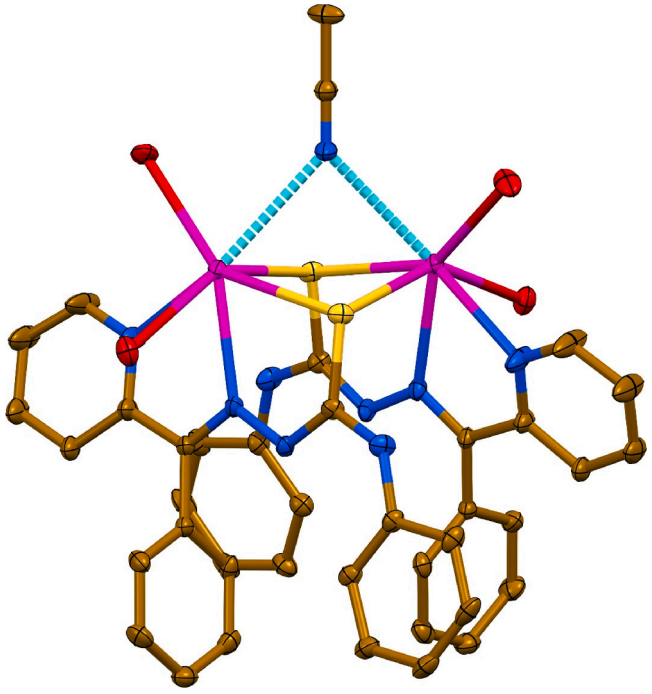

**Fig. 4.** Molecular structure of the dimeric dinuclear cationic building unit $[Pb_2L_2(CH_3CN)]^{2+}$ in the crystal structure of complex **1**·2$H_2O$, built by the Pb•••N tetrel bonds (disordered water molecules and H-atoms were omitted for clarity; only coordinated oxygen atoms of the disordered perchlorate anions are shown). Color codes: C = gold, N = blue, O = red, S = yellow, Pb = magenta; Pb•••N tetrel bond = dashed cyan line.

pivotal role in the stabilization of this complex interacting with both the metal cations with the Pb1•••N5 tetrel bonds of 2.982(7) Å (Fig. 4). The ligand **L** is somewhat flat as supported by the dihedral angles, varying from 3.74 to 11.22° (Table 1), between the mean planes formed by the five-membered metallocycles, Py and Ph(NH) fragments. The other phenyl fragment is close to be orthogonal to the remaining part of **L**, as evidenced from the corresponding dihedral angles ranging from about 78.3(5) to 84.92° (Table 1), a conformation further supported by the C13–H13•••Ph intramolecular interaction formed between one of the *ortho*-H-atoms of the Ph(NH) fragment and the π-system of the central phenyl ring (Table 2). Thus, the cationic species $[Pb_2L_2(CH_3CN)]^{2+}$ is additionally stabilized by a couple of reciprocal C—H•••π-system non-covalent interactions (Fig. 5).

The cationic species $[Pb_2L_2(CH_3CN)]^{2+}$ are glued each other through the formation of reciprocal Pb1•••S1_b tetrel bonds of 3.3873(16) Å, yielding a 1D supramolecular polymeric chain (Fig. 5). Interestingly, the Pb(II) cations interact also with disordered oxygen atoms of the minor occupancy of the perchlorate anions (Table 1). These interactions, being covalent and of 2.764(16) and 2.819(13) Å, are responsible for the formation a 1D covalent polymeric chain (Fig. 5). Alternatively, when oxygen atoms of the major occupancy of the perchlorate anions are considered, three different Pb•••O tetrel bonds of 3.145(9), 3.170(9) and 3.178(8) Å (Table 1) are responsible for the stabilization of a 1D supramolecular polymeric chain. It should be noted, that one of the oxygen atoms of these Pb•••O tetrel bonds is also involved in the formation of a hydrogen bond with the N4–H4N group of the organic ligand **L** (Fig. 5, Table 2). Furthermore, the same hydrogen atom is additionally involved in hydrogen bonding with one of the lattice water molecules (Table 2). Finally, the disordered oxygen atom O3/O13 of the perchlorate anion is involved in the formation of the anion–π-system interaction with the pyridyl fragment (Table 2). Thus, the formation of a 1D supramolecular/covalent polymeric chain from the cationic building units $[Pb_2L_2(CH_3CN)]^{2+}$ and perchlorate anions in the crystal structure of **1**·2$H_2O$ is strongly dictated by a combination of a myriad of Pb•••S and Pb•••N tetrel bonds, and Pb•••O tetrel or Pb–O covalent bonds. As such, the Pb(II) cation is either in an eight-membered $N_3O_2S_3$ coordination environment, constructed from two Pb–N, two Pb–O and two Pb–S covalent bonds, and one Pb•••N and one Pb•••S tetrel bonds, or in a nine-membered $N_3O_3S_3$ coordination environment, constructed from two Pb–N and two Pb–S covalent bonds, and one Pb•••N, three Pb•••O and one Pb•••S tetrel bonds.

The purpose of the DFT theoretical study is to analyse the Pb•••N and Pb•••O non-covalent interactions observed between the dicationic part of **1** and the $CH_3CN$ solvent molecule and perchlorate counterions and to compare them to the Pb•••S bonds responsible for the formation of the dimeric dinuclear cationic species $[Pb_2L_2(CH_3CN)]^{2+}$. To give some insight into the nature of the Pb•••N and Pb•••O contacts, we have used both the QTAIM and NCIplot computational tools since they have been successfully used before to characterize tetrel bonds [21–33]. The distribution of bond critical points and bond paths of the tetrameric assembly (the dicationic part of **1**, the $CH_3CN$ solvent molecule and two perchlorate counterions) is represented in Fig. 6 combined with the NCIplot index. In this representation only the intermolecular bond critical points (also including the coordination Pb–S bonds), bond paths and NCIplot surfaces are shown for clarity. The nitrogen atom of acetonitrile is connected via four bond critical points and bond paths to the $Pb_2S_2$ core, thus forming two N•••Pb and N•••S contacts. Both interactions are further characterized by a NCIplot isosurface located between the nitrogen atom and the whole core. The color of the isosurface is bluish between the nitrogen and lead(II) atoms and green between the nitrogen and sulfur atoms, thus revealing that the N•••Pb interaction is stronger than the N•••S one, taking into consideration the colour scheme used herein (blue and green for strong and weak attractive interactions and red and yellow for strongly and weakly repulsive). This is in line with the value of the charge density at the bond critical points, which is larger for the N•••Pb contact (Table 3). The acetonitrile

**Table 2**
Hydrogen and weak non-covalent bond lengths (Å) and angles (°) for complex **1**·2$H_2O$.[a].

| D–X•••A | *d*(D–X) | *d*(X•••A) | *d*(D•••A) | ∠(DXA) | symmetry code |
|---|---|---|---|---|---|
| N4–H4N•••O1$^{\#1}$ | 0.88 | 2.49 | 3.166(10) | 134 | 3/2 – *x*, *y*, 1 – *z* |
| N4–H4N•••O2W$^{\#2}$ | 0.88 | 2.14 | 3.01(2) | 172 | *x*, 1/2 – *y*, 1/2 + *z* |
| C13–H13•••Ph$^{\#3}$ | 0.95 | 2.92 | 3.784(7) | 152 | *x*, *y*, *z* |
| Cl1–O3•••Py$^{\#3}$ | 1.419(9) | 3.837(12) | 4.177(6) | 93.7(5) | *x*, *y*, *z* |
| Cl1–O13•••Py$^{\#3}$ | 1.551(19) | 3.21(2) | 4.177(6) | 118.4(11) | *x*, *y*, *z* |

[a] Ph = C14–C15–C16–C17–C18–C19.

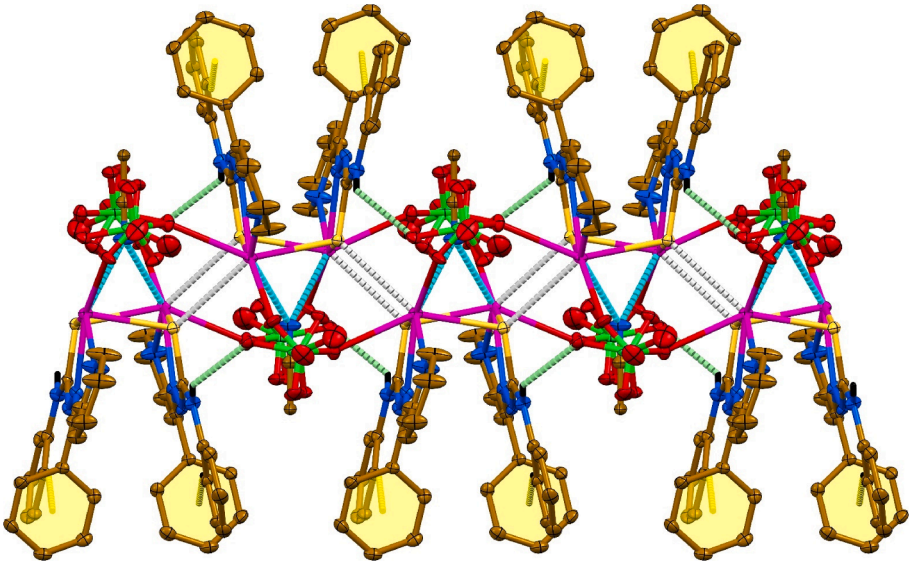

**Fig. 5.** A 1D supramolecular polymeric chain in the crystal structure of complex **1**·2$H_2O$, built by the Pb•••N and Pb•••S tetrel bonds, N–H•••O hydrogen bonds and C–H•••Ph interactions (disordered water molecules and H-atoms, except those involved in N–H•••O hydrogen bonds and C–H•••Ph interactions, were omitted for clarity). Color codes: H = black, C = gold, N = blue, Cl = green, O = red, S = yellow, Pb = magenta; Pb•••N tetrel bond = dashed cyan line, Pb•••S tetrel bond = dashed grey line, N–H•••O hydrogen bond = dashed green line, C–H•••Ph hydrogen bond = dashed yellow line.

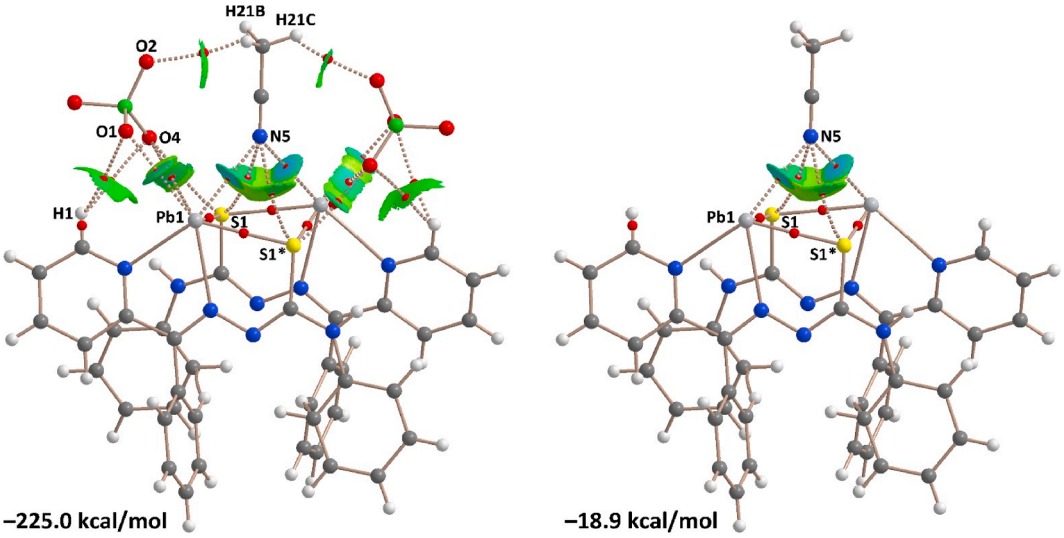


**Fig. 6.** Combined QTAIM (bond and ring critical points are in red and yellow, respectively) and NCIPlot analyses (|RGD| = 0.4, ρ cut-off = 0.04 a.u., color range –0.035 ≤ (sign$\lambda_2$)ρ ≤ 0.035 a.u.) of **1** with (left) and without (right) the perchlorate anions at the PBE0-D3/def2-TZVP level of theory. Only intermolecular interactions are shown.

molecule is also connected to the perchorate anions forming two C–—H•••O interactions characterized by a bond critical point, bond path and small green isosurface interconnecting the hydrogen and oxygen atoms. Each perchlorate anion is connected to the dicationic unit by five bond critical points and bond paths. Two of them correspond to C–—H•••O hydrogen bonds. Two additional ones connect the electron rich O1 and O4 atoms to the electrophilic Pb1, thus establishing a bifurcated Pb•••O contacts. Finally, the combined QTAIM/NCIplot analysis reveals the formation of a S•••O contacts between O4 and S1, characterized by a bond critical point, bond path and green isosurface. The formation energy of this assembly is very large (–225.0 kcal/mol), due to the pure electrostatic attraction between the dinuclear cationic specie $[Pb_2L_2(CH_3CN)]^{2+}$ and both perchlorates, combined with the intricate network of hydrogen bonds, Pb•••O,N and N•••S contacts revealed by the QTAIM/NCIPlot analysis. In case the perchlorate anions are not considered in the calculations, and only the interaction of the

**Table 3**
QTAIM parameters (a.u.) measured at the bond critical points (BCP) labelled in Fig. 6 for the tetrameric assembly of **1**.

| BCP | $\rho_r$ | $\nabla^2\rho_r$ | $V_r$ | $G_r$ | $H_r$ | $E_{dis}$ (kcal/mol) |
|---|---|---|---|---|---|---|
| Acetonitrile | | | | | | |
| S1•••N5 | 0.0093 | 0.0317 | –0.0049 | 0.0064 | 0.0015 | 1.71 |
| Pb1•••N5 | 0.0174 | 0.0497 | –0.0105 | 0.0115 | 0.0010 | – |
| H21C•••O2 | 0.0064 | 0.0256 | –0.0035 | 0.0050 | 0.0015 | 1.09 |
| H21B•••O2 | 0.0043 | 0.0184 | –0.0023 | 0.0034 | 0.0011 | 0.72 |
| Perchlorate | | | | | | |
| Pb1•••O1 | 0.0134 | 0.0338 | –0.0064 | 0.0074 | 0.0010 | – |
| Pb1•••O4 | 0.0101 | 0.0354 | –0.0058 | 0.0074 | 0.0016 | – |
| S1•••O4 | 0.0100 | 0.0406 | –0.0062 | 0.0082 | 0.0020 | 2.16 |
| H1•••O1 | 0.0038 | 0.0122 | –0.0017 | 0.0024 | 0.0007 | 0.53 |
| H1•••O4 | 0.0039 | 0.0155 | –0.0020 | 0.0029 | 0.0009 | 0.63 |
| $Pb_2S_2$ core | | | | | | |
| Pb1•••S1 | 0.0426 | 0.0726 | –0.0310 | 0.0245 | –0.065 | – |
| Pb1•••S1* | 0.0444 | 0.0668 | –0.0312 | 0.0239 | –0.073 | – |

acetonitrile with the dinuclear cationic specie $[Pb_2L_2(CH_3CN)]^{2+}$ is evaluated (Fig. 6), the interaction energy is drastically reduced to –18.9 kcal/mol, thus revealing that the $Pb_2S_2$ core is a good electron acceptor.

We summarize the values of density (ρ), Laplacian of the electron density $\nabla^2\rho$, potential energy density ($V_r$), Lagrangian kinetic energy density ($G_r$) and total energy density ($H_r$) (Table 3), measured at the bond critical points to characterize and analyse the Pb•••O,N,S contacts and C–H•••O H-bonds in compound **1** commented above that are important in the crystal packing of **1**. For the critical points connecting the acetonitrile molecule to the $Pb_2S_2$ core, the QTAIM values reveal that charge and energy densities are larger for the Pb•••N than the Pb•••S contacts in line with the NCIplot index analysis, thus evidencing that the Pb•••N contacts are stronger than the Pb•••S ones. The Laplacian and total energy densities ($H_r$) are positive, thus suggesting the non-covalent nature of these interactions. The C–H•••O contacts present rather small values of charge and energy densities, thus evidencing that these interactions are very weak. For perchlorate, the Pb•••O and S•••O contacts present similar QTAIM parameters, thus suggesting similar strength, in line with the NCIplot isosurface colour observed for these contacts. The QTAIM parameters are smaller for the Pb•••$OClO_3$ than for the Pb•••$NCCH_3$ contacts, thus suggesting stronger interactions for acetonitrile. The C–—H•••O contacts involving the aromatic ring (H1•••O2 and H1•••O4) are also very weak (very small QTAIM parameters at the bond critical points). Table 3 also gathers the QTAIM parameters at the bond critical points that characterize the Pb–S bonds of the $Pb_2S_2$ core. It can be observed that both the density and Laplacian values are significantly higher at these bond critical points than those at the bond critical points that characterize the Pb•••O,N contacts involving the perchlorate and acetonitrile as donors. Moreover, the total energy density values ($H_r$) are negative at the bond critical points that characterize the $Pb_2S_2$ core, which likely indicates some covalent character (semicoordination bonds). In contrast, the $H_r$ values are positive at the rest of bond critical points, thus confirming the non-covalent nature of the Pb•••O and Pb•••N contacts.

In order to estimate the contribution of the hydrogen bonds and S•••N,O contacts we have used the $V_r$ energy predictor. For the hydrogen bonds we have used the equation proposed by Espinosa *et al.* ($E_{dis} = -0.5 \times V_r$) [46]. For the S••• N,O contacts, a different equation proposed in the literature was used [47,48] ($E_{dis} = -0.556 \times V_r$). This equation has been successfully used before in a variety of halogen bonding interactions [49–56]. The obtained results show that the hydrogen bonds involving the acetonitrile are slightly stronger (1.09 kcal/mol and 0.72 kcal/mol) than those involving the aromatic ring (0.63 kcal/mol and 0.53 kcal/mol) (Table 3). This is due to the stronger acidity of the acetonitrile hydrogen atoms that is likely enhanced due to the interaction with the $Pb_2S_2$ core. The S•••O,N contacts are stronger, 1.71 kcal/mol for the one involving acetonitrile and 2.16 kcal/mol for the one involving perchlorate. The contribution of the Pb•••N,O contacts cannot be estimated using the $V_r$ parameter because an appropriate equation has not been proposed yet in the literature. However, the larger $V_r$ values observed for the Pb•••N,O contacts compared to the hydrogen bonds or S•••O,N contacts suggest that they are significantly stronger, in line with the NCIplot analysis discussed above.

## 4. Conclusions

To sum up, we report on a new lead(II) coordination complex $[Pb_2L_2(CH_3CN)(ClO_4)_2]\cdot 2H_2O$ (**1**·$2H_2O$) obtained from a mixture of Pb$(ClO_4)_2\cdot 3H_2O$ and 1-(pyridine-2-yl)benzylidene-4-phenyl-thiosemicarbazide (**HL**) in the methanol/acetonitrile medium. The $^1$H NMR spectroscopy attests that, upon coordination, the parent ligand **HL** is deprotonated. The lead(II) cation is *N,N',S*-coordinated by the tridentate pincer type chelating **L**, yielding a $[Pb_2L_2]^{2+}$ complex cation through a couple of reciprocal bridging Pb–S bonds. The metal centers within this dimeric dinuclear species form two Pb•••N contacts with a bridging acetonitrile molecule leading to the $[Pb_2L_2(CH_3CN)]^{2+}$ building unit. Additional Pb•••S contacts yield a 1D supramolecular polymeric chain. The lead(II) cations interact also with disordered oxygen atoms of the perchlorate anions either through covalent Pb–O bonds or Pb•••O non-covalent bonds. The lead(II) cation can figure out either in an eight-membered $N_3O_2S_3$ coordination environment, realized with two Pb–N, two Pb–O and two Pb–S covalent bonds, and one Pb•••N and one Pb•••S non-covalent bonds, or in a nine-membered $N_3O_3S_3$ coordination environment, constructed from two Pb–N and two Pb–S covalent bonds, and one Pb•••N, three Pb•••O and one Pb•••S non-covalent bonds. The combination of QTAIM and NCIplot index computational tools provide some hints that allows to differentiate non-covalent bonds from classical semicoordination bonds with higher covalent character.

Hence, we have highlighted the crucial role of the lead(II)-derived tetrel bonds on the supramolecular crystal packing of complex **1**·$2H_2O$, and of their dominant role in the formation of an extended structure. We hope that these findings might be of value for researchers when screening an appropriate combination of principal and auxiliary ligands in the design of new metal–organic extended structures.

## Declaration of Competing Interest

The authors declare that they have no known competing financial interests or personal relationships that could have appeared to influence the work reported in this paper.

## Acknowledgements

A. Frontera thanks the MICIU/AEI from Spain for financial support (project number PID2020-115637GB-I00, FEDER funds). This work was supported by state assignment of the Ministry of Science and Higher Education of the Russian Federation (Project Reg. No. 720000Ф.99.1. Б385АА13000). We also thank Ural Interregional World-class Scientific and Educational Center "Advanced Production Technologies and Materials" for the support of this work.

## Appendix A. Supplementary data

Supplementary data to this article can be found online at https://doi.org/10.1016/j.ica.2022.120974.

## References

[1] N.C. Gianneschi, M.S. Masar, C.A. Mirkin, Acc. Chem. Res. 38 (2005) 825–837.
[2] W. Shi, X.-Y. Chen, B. Zhao, A. Yu, H.-B. Song, P. Cheng, H.-G. Wang, D.-Z. Liao, S.-P. Yan, Inorg. Chem. 45 (2006) 3949–3957.
[3] S.R. Batten, N.R. Champness, X.-M. Chen, J. Garcia-Martinez, S. Kitagawa, L. Öhrström, M. O'Keeffe, M. Paik Suh, J. Reedijk, CrystEngComm 14 (2012) 3001–3004.

[4] T. Tao, Y.H. Lei, Y.X. Peng, Y. Wang, W. Huang, Z.X. Chen, X.Z. You, Cryst. Growth Des. 12 (2012) 4580–4587.
[5] M. Du, C.P. Li, C.S. Liu, S.M. Fang, Coord. Chem. Rev. 257 (2013) 1282–1305.
[6] C. Gao, J. Wang, H. Xu, Y. Xiong, Chem. Soc. Rev. 46 (2017) 2799–2823.
[7] R. Arivazhagan, C. Sridevi, A. Prakasam, J. Mol. Struct. 1232 (2021), 129956.
[8] D. Banerjee, P. Yogeeswari, P. Bhat, A. Thomas, M. Srividya, D. Sriram, Eur. J. Med. Chem. 46 (2011) 106–121.
[9] Z. Liu, L.R. Lin, R.B. Huang, L.S. Zheng, Spectrochim. Acta A 71 (2008) 1212–1215.
[10] R.M. Merono, L.M. Taboada, S.G. Granda, Acta Cryst. E 68 (2012) o1945–o1946.
[11] C. Biot, B. Pradines, J. Gut, P.J. Rosenthal, K. Chibale, Bioorg. Med. Chem. Lett. 17 (2007) 6434–6438.
[12] M. Sheikhy, A.R. Jalilian, A. Novinrooz, F.M. Sedeh, J. Biomed. Sci. Eng. 5 (2012) 39–42.
[13] J.N. Reshma, S.D. Avinash, Der. Pharma. Chemica. 5 (2013) 45–49.
[14] C. Shipman Jr., S.H. Smith, J.C. Drach, D.L. Klayman, Antimicrob. Agents. Chemother. 19 (1981) 682–685.
[15] N. Siddiqui, O. Singh, Indian J. Pharm. Sci. 65 (2003) 423–425.
[16] A. Siwek, J. Stefanska, K. Dzitko, A. Ruszezak, J. Mol. Model 18 (2012) 4159–4170.
[17] P.B. Hammond, E.C. Foulkes, Met. Ions Biol. Syst. 20 (1986) 157–200.
[18] J.A. Lewis, S.M. Cohen, Inorg. Chem. 43 (2004) 6534–6536.
[19] P. Mitra, S. Sharma, P. Purohit, P. Sharma, Crit. Rev. Clin. Lab. Sci. 54 (2017) 506–528.
[20] L. Shimoni-Livny, J.P. Glusker, C.W. Bock, Inorg. Chem. 37 (1998) 1853–1867.
[21] G. Mahmoudi, A. Bauza, A. Frontera, Dalton Trans. 45 (2016) 4965–4969.
[22] G. Mahmoudi, A. Bauza, M. Amini, E. Molins, J.T. Mague, A. Frontera, Dalton Trans. 45 (2016) 10708–10716.
[23] G. Mahmoudi, A. Bauza, A. Frontera, P. Garczarek, V. Stilinovic, A.M. Kirillov, A. Kennedy, C. Ruiz-Perez, CrystEngComm 18 (2016) 5375–5385.
[24] G. Mahmoudi, S.K. Seth, A. Bauza, F.I. Zubkov, A.V. Gurbanov, J. White, V. Stilinovic, T. Doert, A. Frontera, CrystEngComm 20 (2018) 2812–2821.
[25] S.K. Seth, A. Bauza, G. Mahmoudi, V. Stilinovic, E. Lopez-Torres, G. Zaragoza, A. D. Keramidas, A. Frontera, CrystEngComm 20 (2018) 5033–5044.
[26] G. Mahmoudi, S.K. Seth, F.I. Zubkov, E. Lopez-Torres, A. Bacchi, V. Stilinovic, A. Frontera, Crystals 9 (2019) 323.
[27] S. Mirdya, S. Roy, S. Chatterjee, A. Bauza, A. Frontera, S. Chattopadhyay, Cryst. Growth Des. 19 (2019) 5869–5881.
[28] A. Bauza, S.K. Seth, A. Frontera, Coord. Chem. Rev. 384 (2019) 107–125.
[29] F. Akbari Afkhami, G. Mahmoudi, F. Qu, A. Gupta, E. Zangrando, A. Frontera, D. A. Safin, Inorg. Chim. Acta 502 (2020), 119350.
[30] G. Mahmoudi, M. Abedi, S.E. Lawrence, E. Zangrando, M.G. Babashkina, A. Klein, A. Frontera, D.A. Safin, Molecules 25 (2020) 4056.
[31] M. Kowalik, J. Masternak, K. Kazimierczuk, B. Kupcewicz, O.V. Khavryuchenko, B. Barszcz, CrystEngComm 22 (2020) 7025–7035.
[32] G. Mahmoudi, A. Masoudiasl, F. Akbari Afkhami, J.M. White, E. Zangrando, A. V. Gurbanov, A. Frontera, D.A. Safin, J. Mol. Struct. 1234 (2021), 130139.
[33] B. Barszcz, J. Masternak, M. Kowalik, Coord. Chem. Rev. 440 (2021), 213935.
[34] R.F.W. Bader, Chem. Rev. 91 (1991) 893–928.
[35] E.R. Johnson, S. Keinan, P. Mori-Sanchez, J. Contreras-Garcia, A.J. Cohen, W. Yang, J. Am. Chem. Soc. 132 (2010) 6498–6506.
[36] Bruker (2007) APEX3, SAINT, v6.28A, Bruker AXS Inc., Madison, Wisconsin, USA, 2016.
[37] Bruker,, SADABS v2012/1, Bruker AXS Inc., Madison, Wisconsin, USA, 2001.
[38] G.M. Sheldrick, Crystal structure refinement with SHELXL, Acta Crystallogr. C 71 (2015) 3–8.
[39] M.J. Frisch, G.W. Trucks, H.B. Schlegel, G.E. Scuseria, M.A. Robb, J.R. Cheeseman, G. Scalmani, V. Barone, G.A. Petersson, H. Nakatsuji, X. Li, M. Caricato, A. Marenich, J. Bloino, B.G. Janesko, R. Gomperts, B. Mennucci, H.P. Hratchian, J.V. Ortiz, A.F. Izmaylov, J.L. Sonnenberg, D. Williams-Young, F. Ding, F. Lipparini, F. Egidi, J. Goings, B. Peng, A. Petrone, T. Henderson, D. Ranasinghe, V.G. Zakrzewski, J. Gao, N. Rega, G. Zheng, W. Liang, M. Hada, M. Ehara, K. Toyota, R. Fukuda, J. Hasegawa, M. Ishida, T. Nakajima, Y. Honda, O. Kitao, H. Nakai, T. Vreven, K. Throssell, J.A. Montgomery, Jr., J.E. Peralta, F. Ogliaro, M. Bearpark, J. J. Heyd, E. Brothers, K.N. Kudin, V.N. Staroverov, T. Keith, R. Kobayashi, J. Normand, K. Raghavachari, A. Rendell, J.C. Burant, S.S. Iyengar, J. Tomasi, M. Cossi, J.M. Millam, M. Klene, C. Adamo, R. Cammi, J.W. Ochterski, R.L. Martin, K. Morokuma, O. Farkas, J.B. Foresman, D.J. Fox, Gaussian 16 (Revision A.03), Gaussian Inc., Wallingford CT, 2016.
[40] S.B. Boys, F. Bernardi, Mol. Phys. 19 (1970) 553–566.
[41] S. Grimme, J. Antony, S. Ehrlich, H. Krieg, J. Chem. Phys. 132 (2010) 154104.
[42] P. Manna, S.K. Seth, M. Mitra, S. Ray Choudhury, A. Bauzá, A. Frontera, S. Mukhopadhyay, Cryst. Growth Des. 14 (2014) 5812–5821.
[43] R.F.W. Bader, J. Phys. Chem. A 102 (1998) 7314–7323.
[44] J. Contreras-Garcia, E. Johnson, S. Keinan, R. Chaudret, J.-P. Piquemal, D. Beratan, W. Yang, J. Chem. Theor. Comp. 7 (2011) 625–632.
[45] T.A. Keith, AIMAll (Version 19.02.13), TK Gristmill Software, Overland Park KS, USA, 2019 (aim.tkgristmill.com).
[46] E. Espinosa, E. Molins, C. Lecomte, Chem. Phys. Lett. 285 (1998) 170–173.
[47] A. Bauzá, A. Frontera, ChemPhysChem 21 (2020) 26–31.
[48] L.E. Zelenkov, D.M. Ivanov, E.K. Sadykov, N.A. Bokach, B. Galmes, A. Frontera, V. Y. Kukushkin, Cryst. Growth Des. 20 (2020) 6956–6965.
[49] L.E. Zelenkov, A.A. Eliseeva, S.V. Baykov, V.V. Suslonov, B. Galmes, A. Frontera, V. Y. Kukushkin, D.M. Ivanov, N.A. Bokach, Inorg. Chem. Front. 8 (2021) 2505–2517.
[50] Y. Torubaev, I.V. Skabitsky, A.V. Rozhkov, B. Galmes, A. Frontera, V.Y. Kukushkin, Inorg. Chem. Front. 8 (2021) 4965–4975.
[51] Z.M. Efimenko, A.A. Eliseeva, D.M. Ivanov, B. Galmes, A. Frontera, N.A. Bokach, V. Y. Kukushkin, Cryst. Growth Des. 21 (2021) 588–596.
[52] A.V. Rozhkov, I.V. Ananyev, A.A. Petrov, B. Galmes, A. Frontera, N.A. Bokach, V. Y. Kukushkin, Cryst. Growth Des. 21 (2021) 4073–4082.
[53] V.V. Suslonov, N.S. Soldatova, D.M. Ivanov, B. Galmes, A. Frontera, G. Resnati, P. S. Postnikov, V.Y. Kukushkin, N.A. Bokach, Cryst. Growth Des. 21 (2021) 5360–5372.
[54] S.V. Baykov, K.K. Geyl, D.M. Ivanov, R.M. Gomila, A. Frontera, V.Y. Kukushkin, Chem. Asian J. 16 (2021) 1445–1455.
[55] E.A. Katlenok, M. Haukka, O.V. Levin, A. Frontera, V.Y. Kukushkin, Chem. Eur. J. 26 (2020) 7692–7701.
[56] A.A. Eliseeva, D.M. Ivanov, A.V. Rozhkov, I.V. Ananyev, A. Frontera, V. Y. Kukushkin, JACS Au 1 (2021) 354–361.